Available online at www.sciencedirect.com

ScienceDirect

Ceramics International 40 (2014) 6109–6113

CERAMICS INTERNATIONAL

www.elsevier.com/locate/ceramint

Low temperature synthesis of semiconducting α-Al_2O_3 quantum dots

K.R. Nemade, S.A. Waghuley*

Department of Physics, Sant Gadge Baba Amravati University, Amravati 444602, India

Received 16 July 2013; received in revised form 14 November 2013; accepted 14 November 2013
Available online 25 November 2013

Abstract

A simple low temperature chemical route, which was based on the reactions of aluminium nitrate and hexamethylenetetramine in aqueous medium at 473 K for 36 h, was proposed for the synthesis of α-Al_2O_3 quantum dots (QDs). The characterisation results from X-ray diffraction, Fourier transform infrared spectroscopy and transmission electron microscopy along with selected area diffraction pattern are revealed the formation of α-Al_2O_3. Ultra-violet spectra indicated that the as-synthesised α-Al_2O_3 has a direct band gap of about 3.6 eV and also disclosed semiconducting behaviour of α-Al_2O_3 QDs using defect chemistry.
© 2013 Elsevier Ltd and Techna Group S.r.l. All rights reserved.

Keywords: B. Defects; Semiconductor; Quantum dots; Chemical route

1. Introduction

Among many metal oxides, aluminium oxide (Al_2O_3) is currently one of the most useful oxide ceramics [1]. Okubo et al. [2] reported the Al_2O_3/InN composite material. This material is one of the most promising materials for high-speed electronic devices because of its high electron mobility [3] and high saturation drift velocity [4]. French et al. studied the optical and electronic properties of α-Al_2O_3 by using the vacuum ultraviolet spectroscopy, confirms the insulating nature of Al_2O_3 due to its large band gap of the order 14 eV [5]. Mirjalili et al. reported synthesis of nanocrystalline α-Al_2O_3 at 1473 K for about 1 h by the sol–gel method [6]. Weber et al. discussed the presence of band gap in Al_2O_3 on the basis of native defects [7]. Li et al. [8] reported the synthesis of ultrafine α-Al_2O_3 powder by a simple aqueous sol–gel process at 1273 K. Zaki et al. [9] prepared highly pure α-Al_2O_3 nanoparticles at relatively low temperatures 1198 K by using the Pechini method.

Here, a relatively simple, efficient and low temperature method has been developed to synthesis α-Al_2O_3 quantum dots (QDs). The novelties of present work are we achieved α-Al_2O_3 phase at relatively low temperature (473 K) than reported in the literature and semiconducting band gap for α-Al_2O_3.

2. Experimental methods

All chemicals used were of analytical grade (SD fine, India). The sample was prepared with deionized water of resistivity not less than 18.2 MΩ/cm. The aluminium nitrate and hexamethylenetetramine (HMT) were used for the synthesis of Al_2O_3 QDs. In a typical synthesis, 1 M aluminium nitrate was mixed with 1 M HMT in 30 ml deionized water under magnetic stirring for 15 min at room temperature. Subsequently, obtained product kept for a centrifuge operating at 3000 rpm for 30 min. After this procedure, solution was separated into two gradations. At the bottom a white layer of Al_2O_3 QDs observed and over it more transparent and dispersed layer appeared. This centrifuged precipitate was collected through cellulose nitrate filter paper. The filtrate was dried at room temperature for overnight in vacuum chamber and then sintered at 473 K for 36 h. After sintering the synthesised material appears white coloured powder in visible light. The reaction is shown in Eq. (1).

$$Al(NO_3)_2 + C_6H_{12}N_4 \rightarrow Al_2O_3 + C_6N_6 + 6H_2O \quad (1)$$

X-ray diffraction (XRD) patterns were recorded using a Rigaku miniflex-II diffractometer with CuKα radiation in the

*Corresponding author. Tel.: +91 9423124882.
E-mail address: sandeepwaghuley@sgbau.ac.in (S.A. Waghuley).

0272-8842/$ - see front matter © 2013 Elsevier Ltd and Techna Group S.r.l. All rights reserved.
http://dx.doi.org/10.1016/j.ceramint.2013.11.062

range 20–70°. The morphology and grain size of the sample was observed by using (transmission electron microscopy along with selected area diffraction pattern) TEM-SADP (JEOL-1200ex). The ultraviolet–visible (UV–vis) spectrum recorded on Perkin Elmer UV spectrophotometer in the range 300 − 450 nm in solution of Al_2O_3 QDs dispersed in double distilled water. The Fourier transform infrared (FTIR) spectrum was recorded on Shimadzu (Model-8201) spectrophotometer. The fluorescence analysis was done on FL Spectrophotometer (Model: HITACHI, F-7000). The thermo-gravimetric–differential thermal analysis (TG–DTA) was obtained with a Shimadzu DTG-60h thermal analyser under nitrogen atmosphere.

3. Results and discussion

The XRD pattern of the final product is shown in Fig. 1. α-Al_2O_3 has a trigonal structure with space group R3c and is commonly described in terms of hexagonal Miller–Bravais indices with $a=4.76$ Å and $c=12.99$ Å [10,11]. The diffraction peaks appears at various 2θ positions, exactly indexed to the formation of this compound (PDF-01-081-1667). No other peaks for impurities were detected. The average crystallite size was calculated from diffraction peaks using the Debye–Scherrer equation, which was found to be 4.2 nm [12].

The surface topography of Al_2O_3 QDs was examined through TEM. Fig. 2 shows the TEM image of Al_2O_3 QDs. The distribution of grains are of irregular shapes through all the regions of image. The inset is the corresponding SAED pattern of Al_2O_3 QDs. The diffraction planes were obtained from XRD analysis, are consistent with the rings on the diffraction pattern.

Fig. 3(a) shows UV visible absorption spectrum of α-Al_2O_3 QDs and it clearly shows an intense band-to-band absorption in the ultra violet region. Band gap value was determined by extrapolation of the linear portion of $(\alpha h\nu)^{1/2}$ curve versus the photon energy ($h\nu$) as 3.6 eV as shown in Fig. 3(b). The observation of blue shift in band gap shows the formation of smaller sized α-Al_2O_3 QDs and the presence of strong quantum confinement effect [13–15].

As the quantum confinment effect present in α-Al_2O_3 QDs, its radius was estimated by using the hyperbolic band model (HBM). The QDs radius was estimated from 350 nm intense absorption using Eq. 1 [14]

$$R = \sqrt{\frac{2\pi^2 h^2 E_{bulk}}{m^*(E_{nano}^2 - E_{bulk}^2)}} \quad (2)$$

where $E_{bulk}=2.6$ eV is the bulk band gap of Al_2O_3 [16], $E_{nano}=3.6$ eV is the band gap of Al_2O_3 QDs, m^* is the effective mass of electron in Al_2O_3 ($m^*=0.28m_0$) [17]. The QDs radius was found to be 2.14 nm, hence particle size is $2R=4.28$ nm.

This value of band gap shows Al_2O_3 QDs possesses semiconducting behaviour. This could be due to the presence of different sub-energy levels in the bandgap, which are related to surface defects. This semiconducting behaviour can be explained using the defect chemistry. The band gap is controlled, fundamentaly, by the concentration of defects. Defects ionised to some extent, at room temprature, by thermal

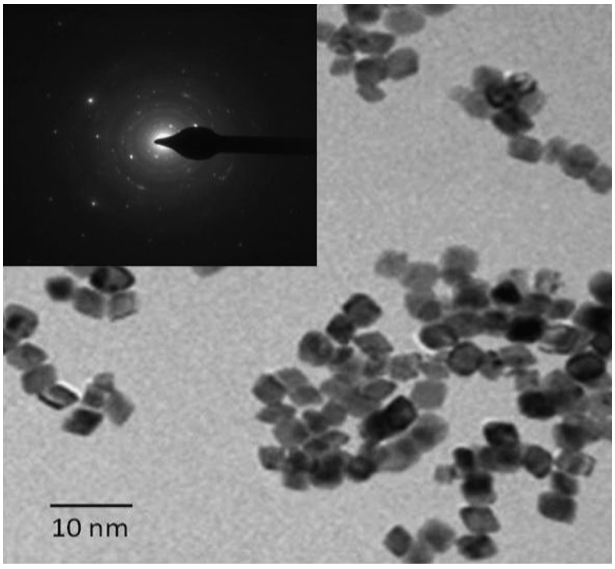

Fig. 2. TEM image of as-synthesized α-Al_2O_3 QDs and the inset shows SADP pattern.

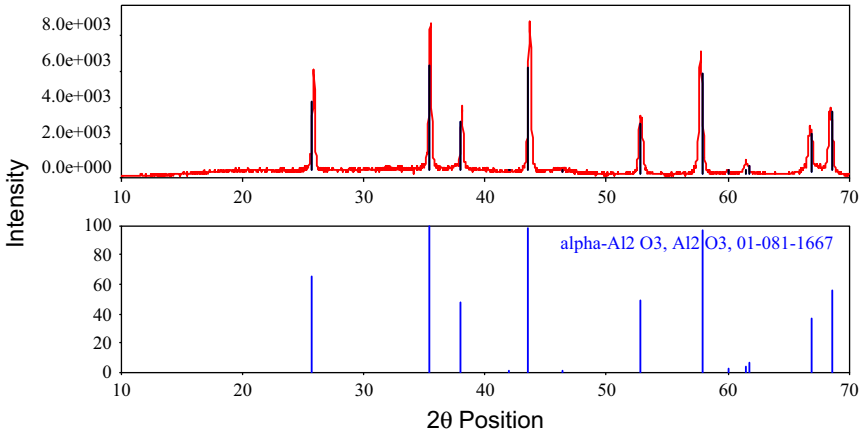

Fig. 1. XRD of as-synthesised α-Al_2O_3 QDs.

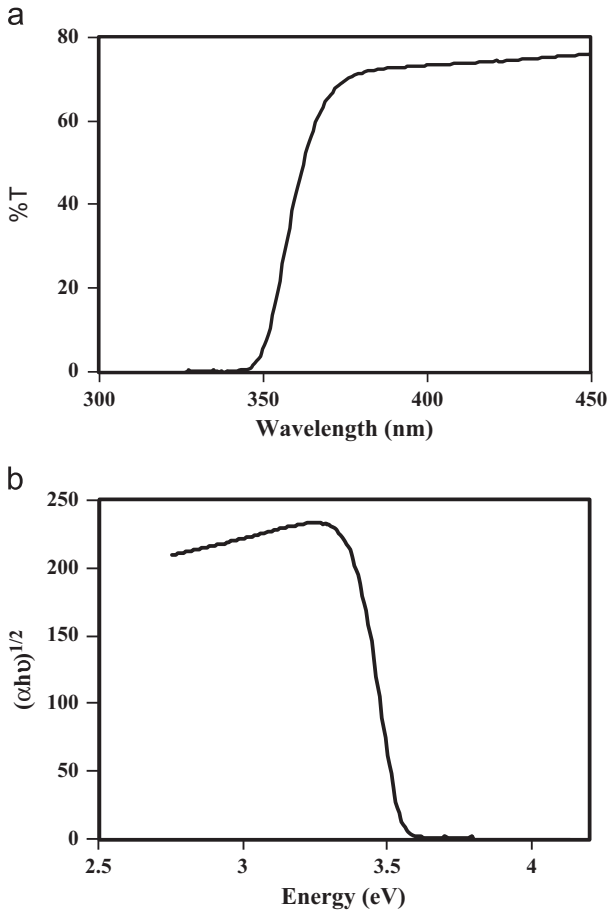

Fig. 3. (a) UV–vis spectrum and (b) plot of $(\alpha h\nu)^{1/2}$ as a function of photon energy of Al_2O_3 QDs dispersed in aqueous medium.

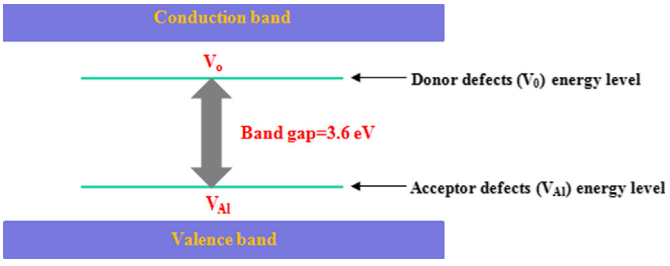

Fig. 4. Energy levels of donor defects (V_0) and acceptor defects (V_{Al}). As these defects readily ionised at room temperature, therefore resultant band gap of Al_2O_3 QDs at room temperature is 3.6 eV.

fluctuations and hence electrons may promoted into the conduction band. In the metal oxide, vacant oxygen sites played the role of defects. In neutral state they contain two electrons one of which is readily ionised [18]. This electron is easily promoted into conduction band even at room temprature. This is one of the possible reasons for the mearging of insulating band gap of Al_2O_3 into semiconducting region. The electronic energy levels of donor and acceptor defects are shown in Fig. 4. The Kroger Vink notations are used to explain this energy levels, where V=vacancy, O=oxygen, Al=Aluminium. The Al interstitials and oxygen vacancies are known to be the predominant ionic defects. This shows that the donor defects (oxygen vacancies) create their energy level below the conduction band, whereas the acceptor defects (Al interstitials) create energy level above the valence band [19]. The Al interstitials/defects arise from the Frenkel reaction whereas the oxygen vacancies/defects are from the Schottky reaction [19].

Fig. 5(a) reveals the FTIR spectrum of α-Al_2O_3 QDs. In Fig. 2, there is transmission band entered at about 3250 cm^{-1}, characteristic of hydrogen bonded –O–H of the adsorbed water. The band at 1108 cm^{-1} is corresponding to the phonon lengthways stretching band of Al_2O_3 [20,21], while the band at 500–1000 cm^{-1} can be interpreted to the bending stretching band of Al–O [22]. The transmission band at 1631 cm^{-1} is the characteristic of the bending stretching of the adsorbed H_2O, while the bands at 2358 and 2260 cm^{-1} are the characteristics of the adsorbed CO_2. The FTIR peaks of precursor molecules that is HMT such as 2958, 2882, 1462, 1358, 1234, 1010, 816, 669 cm^{-1} do not appear notably [23].

The size tunable absorption and emission properties of QDs are extremely valuable for quantum confinement analysis. Due to this reason, QDs are said to be fluorescent nanocrystals [14–24]. In the present work, QDs shows the emission of intense blue luminescence under the irradiation by 254 nm at room temperature. In order to calculate particle size, a fluorescence measurement was made from 275 to 625 nm and displayed in Fig. 5(b). The peak value of emission was observed at 383 nm, which is assigned to the presence of defects. This value demonstrates the concentration of defects responsible for emission. This value is used for the manipulation of quantum dots' size from effective mass approximation (EMA).

The optical band gap and particle size are correlated with Eq. 2 [25].

$$E_g = E_{bulk} + \frac{h^2}{8r^2}\left(\frac{1}{m_e^*} + \frac{1}{m_h^*}\right) - \frac{e^2}{4\pi\varepsilon_0\varepsilon_r\gamma_e} \quad (3)$$

where r is the radius of the particle, γ_e=20 nm is the Bohr exciton radius of Al_2O_3 [26], E_{bulk} is the bulk band gap, ε_r is the relative dielectric constant, ε_0 is the dielectric constant of air, $m_e^*=0.28m_0$ [17] effective mass of electron in Al_2O_3 QDs and $m_h^*=0.38m_0$ is effective mass of hole in Al_2O_3 QDs [27]. These calculations are resulted in the radius of QDs. It was found that r=1.92 nm. Thus, QD size is $2r$=3.84 nm. The HBM and EMA studied using UV–vis and fluorescence spectroscopy respectively confirm the presence of quantum confinement in Al_2O_3 QDs.

Fig. 5(c) offers a clear thermal analysis of the α-Al_2O_3 QDs. Endothermic peaks at 397 and 437 K correspond to the decomposition remaining contents of α-Al_2O_3 QDs, i.e. $Al(OH)_3$ and AlO(OH) respectively. The exothermic peak at 418 K is accompanied by a drastic mass loss in the temperature range 340–500 K. The mass loss (1.97 mg) associated with these exothermic and an endothermic process is about 87%. This drastic mass loss attributed to the limited number of possible slip systems in α-Al_2O_3 behaves in a brittle manner at lower temperatures. Three dislocation slip systems have commonly been identified for α-Al_2O_3 above its brittle–ductile transition temperature of about 400 K. Deformation in α-Al_2O_3

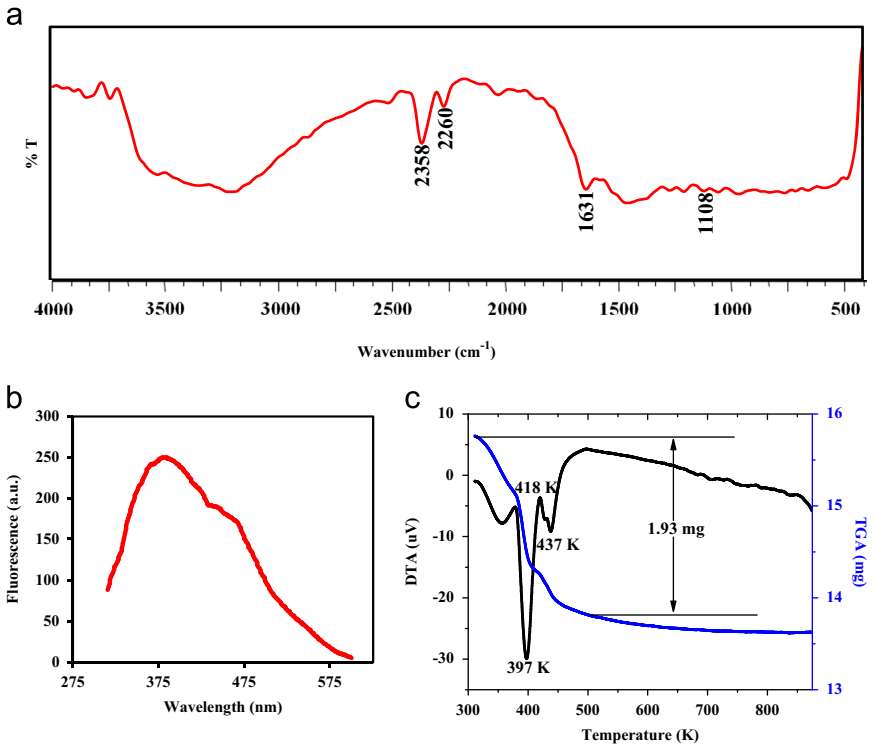

Fig. 5. (a) FTIR spectrum, (b) fluorescence spectrum, and (c) TG–DTA of α-Al_2O_3 QDs.

Table 1
Particle size determined from XRD, TEM, UV–vis and fluorescence analysis.

Characterization technique	Particle size (nm)
XRD	4.2
TEM	4
UV–vis	4.28
Fluorescence	3.84

crystals strongly appears in temperature range 673–1073 K suggests that prismatic slip results in mass loss [28].

The particle sizes computed from the above discussed spectroscopy are in good agreement with XRD and TEM analyses. The particle sizes determined using the XRD, TEM, UV–vis and fluorescence analyses are listed in Table 1. These values are in good agreement with each other. The small deviation in particle size computed from XRD and TEM with UV–vis and fluorescence analyses may be due to the limitation of HBM and EMA i.e. particles are strictly spherical.

4. Conclusions

Texture characterisation was performed using XRD, TEM-SADP, FTIR and TG–DTA, clearly suggested the formation of α-Al_2O_3 QDs via chemical route at much lower temperature than the conventional methods. Similarly, an intrinsic characteristic of quantum dots that is the presence of quantum confinement is confirmed by UV–vis spectroscopy. The as-synthesised QDs had a direct band gap of about 3.6 eV, and exhibited a defect-induced strong emission at 383 nm. The semiconducting behaviour of α-Al_2O_3 QDs discussed effectively by using defects chemistry.

Acknowledgements

Authors are very much thankful to Head, Department of Physics Sant Gadge Baba Amravati University, Amravati for providing necessary facilities.

References

[1] A.I.Y. Tok, F.Y.C. Boey, X.L. Zhao, Novel synthesis of Al_2O_3 nanoparticles by flame spray pyrolysis, J. Mater. Process. Technol. 178 (2006) 270–273.
[2] K. Okubo, A. Kobayashi, J. Ohta, H. Fujioka, M. Oshima, Polarity dependence of structural and electronic properties of Al_2O_3/InN interfaces, Appl. Phys. Express 4 (2011) 091002–091005.
[3] T.B. Fehlberg, G.A. Umana-Membreno, B.D. Nener, G. Parish, C.S. Gallinat, G. Koblmuller, S. Rajan, S. Bernardis, J.S. Speck, Characterisation of multiple carrier transport in indium nitride grown by molecular beam epitaxy, J. Appl. Phys. 45 (2006) L1090–L1092.
[4] K.T. Tsen, C. Poweleit, D.K. Ferry, H. Lu, W.J. Schaff, Observation of large electron drift velocities in InN by ultrafast Raman spectroscopy, Appl. Phys. Lett. 86 (2005) 222103–222106.
[5] R.H. French, Electronic structure of α-Al_2O_3, with comparison to AlON and AlN, J. Am. Ceram. Soc. 73 (1990) 477–489.
[6] F. Mirjalili, H. Mohamad, L. Chuah, Preparation of nano-scale α-Al_2O_3 powder by the sol–gel method, Ceramics – Silikaty 55 (2011) 378–383.
[7] J.R. Weber, A. Janotti, C.G. Van de Walle, Native defects in Al_2O_3 and their impact on III–V/Al_2O_3 metal-oxide-semiconductor-based devices, J. Appl. Phys. 109 (2011) 033715–033722.
[8] J. Li, Y. Pan, C. Xiang, Q. Ge, J. Guo, Low temperature synthesis of ultrafine α-Al_2O_3 powder by a simple aqueous sol–gel process, Ceram. Int. 32 (2006) 587–591.

[9] T. Zaki, K.I. Kabel, H. Hassan, Preparation of high pure α-Al_2O_3 nanoparticles at low temperatures using Pechini method, Ceram. Int. 38 (2012) 2021–2026.
[10] J. Cadoz, B. Pellissier, Influence of three-fold symmetry on pyramidal slip of alumina single crystal, Scr. Metall. 10 (1976) 597–600.
[11] S. Ruppi, Enhanced performance of α-Al_2O_3 coatings by control of crystal orientation, Surf. Coat. Technol. 17 (2008) 4257–4269.
[12] K.R. Nemade, S.A. Waghuley, LPG sensing application of graphene/Bi_2O_3 quantum dots composites, Solid State Sci. 22 (2013) 27–32.
[13] K.R. Nemade, S.A. Waghuley, LPG sensing application of graphene/CeO_2 quantum dots composite, AIP Conf. Proc. 1536 (2013) 1258–1259.
[14] K.R. Nemade, S.A. Waghuley, UV–vis spectroscopic study of one pot synthesized strontium oxide quantum dots, Results Phys. 3 (2013) 52–54.
[15] K.R. Nemade, S.A. Waghuley, Carbon dioxide gas sensing application of graphene/Y_2O_3 quantum dots composite, Int J. Mod. Phys.: Conf. Ser. 22 (2013) 380–384.
[16] V. Rose, R. Franchy, The band gap of ultrathin amorphous and well-ordered Al_2O_3 films on CoAl(100) measured by scanning tunneling spectroscopy, J. Appl. Phys. 105 (2009) (07C902–07C905).
[17] M.L. Huang, Y.C. Chang, C.H. Chang, T.D. Lin, J. Kwo, T.B. Wu, M. Hong, Energy-band parameters of atomic-layer-deposition Al_2O_3/InGaAs heterostructure, Appl. Phys. Lett. 89 (2006) 012903–012906.
[18] J.M. Herbert, Ceramic Dielectrics and Capacitors, Gordon and Breach Science Publishers, New york, 1985.
[19] L.S. Mende, J.L. MacManus-Driscoll, ZnO – nanostructures, defects, and devices, Mater. Today 10 (2007) 40–48.
[20] X. Ye, J. Sha, Z. Jiao, L. Zhang, Size effect on structure and infrared behaviour in nanocrystalline magnesium oxide, Nano-Struct. Mater. 8 (1997) 945–951.
[21] C. Zheng, X. Zhang, J. Zhang, K. Liao, Preparation and characterization of VO_2 nanopowders, J. Solid State Chem. 156 (2001) 274–280.
[22] Y. Wang, C. Suryanarayana, L. An, Phase transformation in nanometer-sized c-Al_2O_3 by mechanical milling, J. Am. Ceram. Soc. 3 (2005) 780–783.
[23] B.B. Garcia, D. Liu, S. Sepehri, S. Candelaria, D.M. Beckham, L. W. Savage, G. Cao, Hexamethylenetetramine multiple catalysis as a porosity and pore size modifier in carbon cryogels, J. Non-Cryst. Solids 356 (2010) 1620–1625.
[24] A.M. Smith, H. Duan, A.M. Mohs, S. Nie, Bioconjugated quantum dots for In vivo molecular and cellular imaging, Adv. Drug Deliv. Rev. 60 (2008) 1226–1240.
[25] J.P. Reddy, S. Kashayap, A.K. Paul, Synthesis and optical characterization of ZnO quantum dots and nanorods, Adv. Sci. Eng. Med. 4 (2012) 222–224.
[26] N.O. Dantas, P.M.N. Paula, R.S. Silva, V. Lopez-Richard, G.E. Marques, Radiative versus nonradiative optical processes in PbS nanocrystals, J. Appl. Phys. 109 (2011) 024308–024312.
[27] E.J. Medvedeva, E.N. Teasley, M.D. Hoffman, Electronic band structure and carrier effective mass in calcium aluminates, Phys. Rev. B 76 (2007) 155107–155113.
[28] K.P.D. Lagerlof, A.H. Heuer, J. Castaing, J.P. Riviere, T.E. Mitchell, Slip and twinning in sapphire (α-Al_2O_3), J. Am. Ceram. Soc. 77 (1994) 385–397.